Distribution and Ventilation of Deep Ocean Heat along the Western Antarctic Peninsula

by
[1]Douglas G. Martinson

[1]Lamont-Doherty Earth Observatory and
Department of Earth and Environmental Sciences, Columbia University
Palisades, NY 10964

Submitted to Science (2/16/05)

Abstract:

The Antarctic Peninsula (AP) shows the fastest regional warming on Earth, with rapidly melting glaciers and dramatic changes in sea ice and marine ecosystems. The role of the ocean in these changes is still uncertain. The distribution and ventilation of ocean heat on the western-AP shelf is described using 10 years of annual ocean data to provide a foundation to better evaluate the ocean's role in these and other changes. "Warm" ocean water, delivered by Antarctic Circumpolar Current flooding of the continental shelf, is mapped across the shelf. Frequent flooding is responsible for a winter-average vertical ocean heat flux of ~28Wm^{-2}; ocean destabilization forming bottom water is a distinct possibility.

Report Text:

Recent rapid regional warming over the Antarctic Peninsula (AP) is among the fastest documented on Earth (*1*). This warming has important implications for sea level because it is driving fast retreat of ice shelves and glaciers (*2-4*), especially near the base of the AP and farther southwest where large buttressing ice shelves appear to be rapidly thinning (*3*). Other studies (*5,6*) document retreating Amundsen and Bellingshausen sea ice cover and glacial ice. Stammerjohn (*7*) shows a pre-1988 perennial ice cover of the western AP (wAP) coastal areas switching to a seasonal ice cover post-1988. While the focus of this rapid melting has been related to the warming air temperatures (*8-10*) with the underlying processes elucidated (*11*), recent studies suggest that warm (relative to freezing) ocean waters may play a bigger role than previously expected (*12,13*). The delivery and distribution of ocean heat on the continental shelf of the wAP is addressed to establish a foundation against which to further evaluate the ocean's role in these and other changes (such as marine ecosystem changes (*14*) and those indicated from recent high-resolution sediment cores suggesting alternating episodes of warm versus cold shelf bottom waters (*15*)).

This ocean foundation is established by focusing on: (1) the local distribution of the most voluminous Southern Ocean source of ocean heat and nutrients: Circumpolar Deep Water (CDW) transported by the Antarctic Circumpolar Current (ACC), and (2) the means of ocean heat ventilation, including the likelihood of polynya formation in coastal waters that would vent extensive ocean heat to the winter atmosphere and possibly lead to other effects that can amplify local impacts (*16*).

This study uses 10 years of annual data collected in the nominal sampling grid (Figure 1) by the Palmer Long Term Ecological Research (LTER) project (*17*) since 1993, supplemented by other relevant data, as discussed with Figure S1. The grid, predominantly overlying the continental shelf, occupies a region ~300 km in cross-shelf width running ~500 km along the wAP. Here, the ACC flows along the shelf/slope break, as it does throughout the entire region (*18*) (Figure 1A). Because the ocean heat (in the CDW) is supplied via the ACC, its close proximity to the continental shelf facilitates delivery of the warm water to the shelf and glacial termini. Since the ACC skirts the shelf throughout the region the ACC-shelf interactions in the LTER sample grid may be representative of those in similar regions, including to the southwest (where larger, more voluminous glaciers and ice shelves are rapidly thinning). However, this SW region has a wider shelf and may possess an eastwind drift, demanding additional *in situ* data to test this relationship.

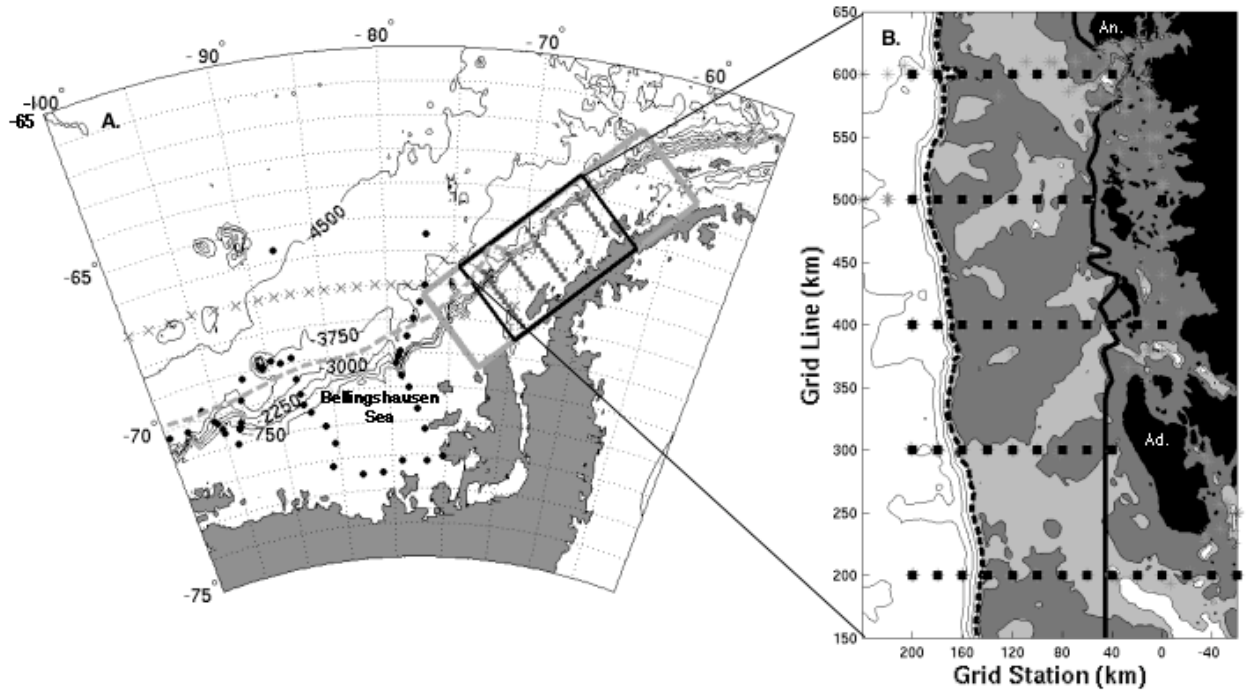

Figure 1: A. Study region along wAP and nominal sampling grid (bold black box) imbedded in bigger full grid (bold grey box) with labeled contoured bathymetry (750 m intervals) and climatological southern edge of ACC (dashed grey line); hydrographic stations (small squares), the WOCE S04P section (grey x's), NBP94-02 section (solid dots) on Bellingshausen Sea shelf (and Amundsen Sea shelf off map to west). B. Nominal sampling grid; bathymetry shaded (white ≥750m, 750< light-grey ≤450m, dark-grey <450m) and contoured (≥1500m @750m intervals); islands labeled: An. = Anvers Island, Ad. = Adelaide Island; continental slope-shelf break indicated by dashed bold line (slope to left) and shelf- coastal sub-regions separated by solid bold line; standard station locations (small squares) as well as numerous others occupied (*) are indicated; grid lines (ordinate) and grid stations (abscissa) are indicated and labeled.

Fundamental to this analysis is the relationship of shelf water masses to those of the ACC which transports CDW. Key water masses, as they appear in the austral *summer* wAP region, are shown in Figure 2. Gordon (*19*) distinguishes between Upper and Lower CDW, noting that these are distinguished by temperature (UCDW) and salinity (LCDW) maxima; the latter is absent in the wAP. Over the broad circumpolar belt the UCDW spans a considerable range in temperature (T; note that most of the analyses involve shallow depths, so potential temperature (θ) is only presented when the deep profiles are shown, as in Figure 2) and salinity (S) (salinities are unit-less, but compatible with ppt (*20*)). To relate the shelf waters to those being transported by the ACC, a restricted definition of UCDW is adopted: θ_{max} water as it appears in the ACC core immediately offshore. The data used for this are the WOCE S04P section (February, 1992; Figure S2), focusing on profiles taken in deep water within 1000 km of the wAP shelf, and the NBP94-02 section (*21*) over the Bellingshausen Sea slope (March 1994). θ_{max} water at these stations occupy a more restricted area in T–S space, shown by the UCDW box in Figures 2A and S3, as $1.70 \leq \theta \leq 2.13^{\circ}$ C; $34.58 \leq S \leq 34.75$ (hereafter, referred to as "ACC-core UCDW").

When ACC-core UCDW is swept onto the shelf, mixing cools it to form modified UCDW (M-UCDW). Unmodified UCDW incursions survive short distances on the shelf (Figure S5). These incursions are consistent with dynamic topography calculations in the grid in numerous years and with LTER ADCP current observations (*22*). The southern limit of UCDW and the Southern ACC Front (SACCF; southern limit of ACC indicated by abrupt shoreward uplift of the isopycnals) coincide in this region (*23*) and lie (climatologically) at the shelf-slope break.

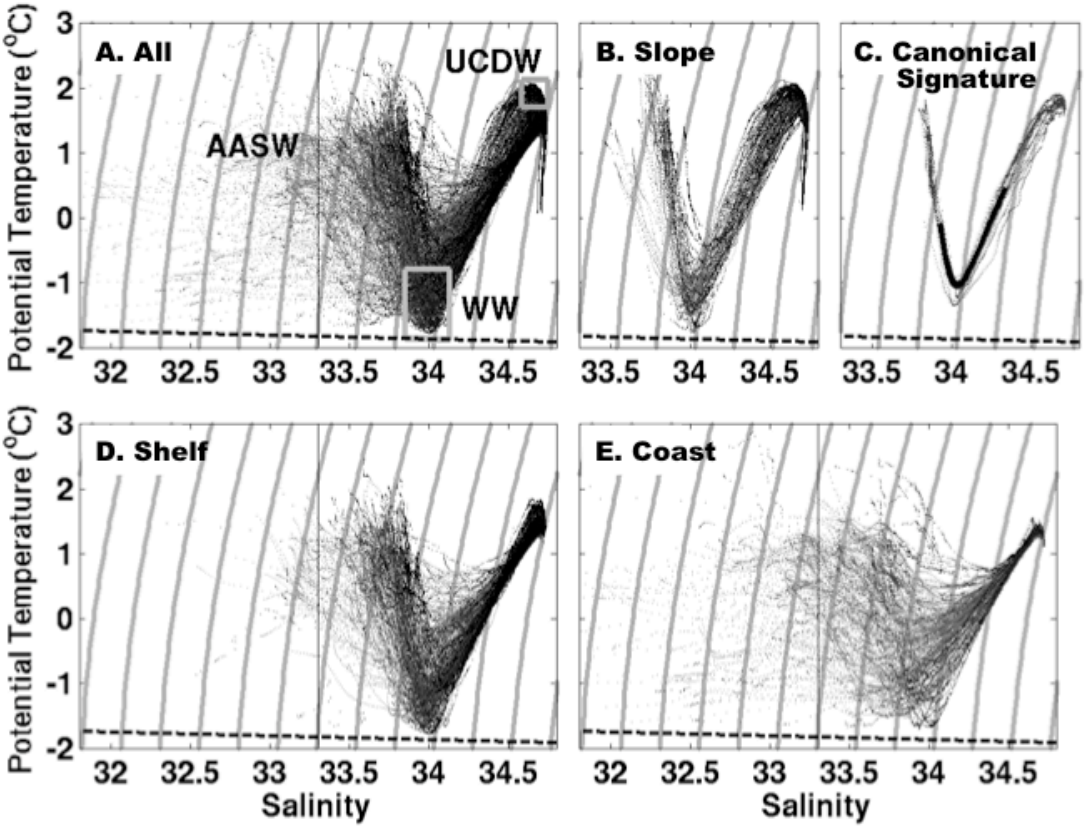

Figure 2: (A) Decade of summer θ–S scatter plots, with key water masses, as they appear in the wAP region indicated and labeled (UCDW = ACC-core Upper Circumpolar Deep Water; WW = Winter Water, the remnant winter mixed layer water; AASW = Antarctic Surface Water in summer). Regional bathymetry serves as a geographic sieve, thus summer θ–S plots are separated according to sub-regions: (B) Slope; (D) Shelf; and, (E) Coastal waters. (C) Canonical signature (bold line) of ACC slope-water for 1993 slope data. Isopycnals appear as grey lines across θ-S space. All graphs use common θ and S scales (though S-range is restricted for B and C); freezing line is dashed line across inside bottom; data shaded according to year (1993 lightest — 2002 darkest).

The modification of UCDW on the shelf hinders the tracking of its paths each year, but fortunately "ACC slope-water" (ACC water flowing over the continental slope, carrying ACC-core UCDW) displays a locally identifiable upper-ocean signature through the upper half of the permanent pycnocline. This water is characterized by a sharp V shape and reduced scatter in θ-S space (Figure 2B), relative to that in the shelf and coastal waters. This is used to define a unique θ-S signature of the ACC slope-water by creating a "canonical" shape of the upper-ocean waters of the continental slope for each year (serving as a proxy for that year's ACC-core UCDW water;

Figure 2C). The V-shape is isolated by focusing on those waters cooler than 0˚ C in the seasonal pycnocline and cooler than 0.5˚ C in the permanent pycnocline. The canonical shape is defined as the gravest mode (always describing >95% of the observed variance) of an empirical orthogonal function (EOF) analysis on the θ-S plots (using θ as a function of S) for all slope stations each year. Defining a new canonical shape for each year allows for differences due to local/regional and interannual variability.

For each year, the canonical shape in θ-S space is correlated to the data at each station across the grid. Maps of the coefficient of determination (R^2) as a function of station location and year (Figure 3) provide an indication of the annual summer distribution (flooding) of ACC slope-water across the shelf. R^2 describes the fraction variance captured at the grid station. Comparing stations taken in January and March of 1993 shows that values of $R^2 \geq 0.7$ (all shades of red in Figure 3) are a reasonable indication that the station has been recently flooded (within 3 months) by ACC slope-water.

Two characteristics of these maps stand out: (1) the shelf is regularly bathed in ACC slope-water (providing warm deep water), (2) the spread of ACC slope-water across the shelf shows a couple of regular paths. The water often appears to flood the shelf from the southwest, as expected for northeastward flowing ACC (*22,24*), though sometimes it appears to enter from the slope (e.g., 1993, 1997). The northeastern extent of the grid near Anvers Island ("Anvers region") is rarely bathed in ACC slope-water, perhaps reflecting its complex bathymetry/coastline or southward flowing Bransfield Strait water (*25*). The UCDW of the ACC slope-water flooding has temperature averaging 1.9˚C and salinity averaging 34.67. Mixing leads to M-UCDW averaging 1.4˚ C, 34.68 over the shelf and 1.2˚ C, 34.63 in the coastal regions confirming the need to use the canonical signature to track the water across the shelf.

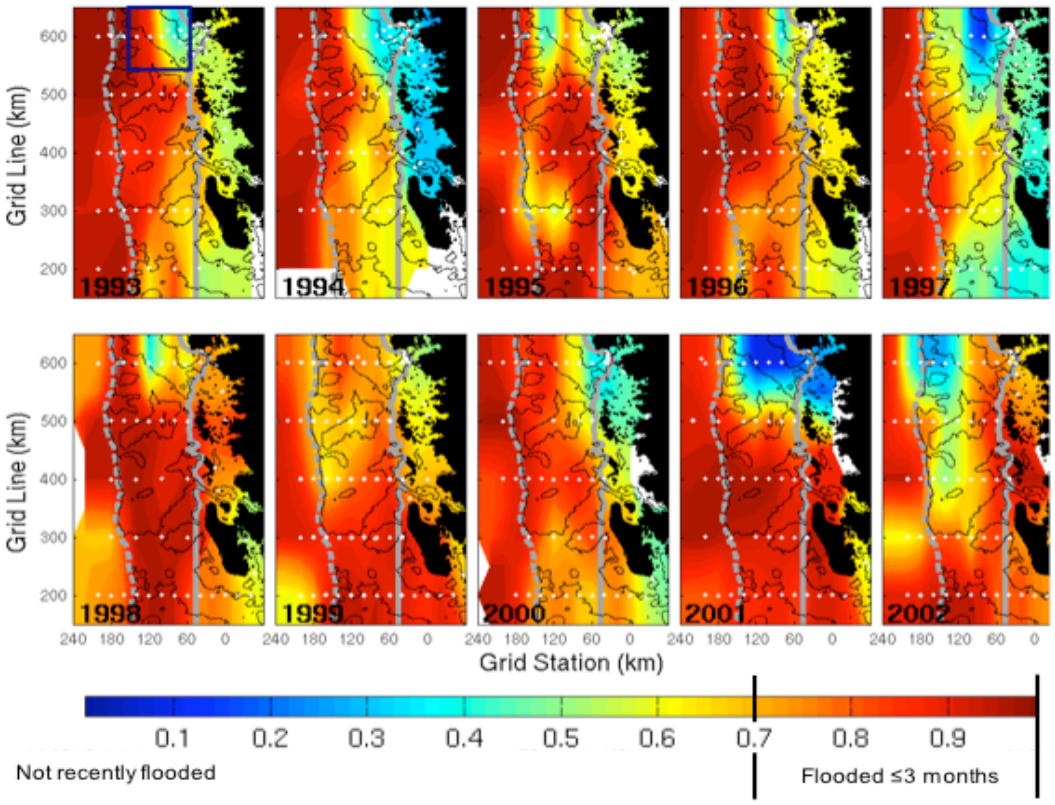

Figure 3: Coefficient of determination (R^2) showing correlation (as fraction of described variance) of local θ-S signature to ACC slope-water θ-S signature. All shades of red indicate presence of recently delivered ACC slope-water (within ~3 months), which appears to flood most of the sampling grid, most years. Blue box in upper center of 1993 map is "Anvers region" showing minimal flooding. 450m depth contour shown.

The regular grid flooding resupplies sub-pycnocline warm deep water and makes heat available to the surface. The warm water provides the primary source of stability against convective overturn (*25*) in winter by reducing sea ice growth and its destabilizing brine. Exhaustion of this heat (or extensive sea ice growth in its presence) could lead to overturn and polynya formation with a 20-fold increase in the air-sea heat flux, requiring consideration of how the heat is vented.

Martinson and Iannuzzi (*26*) estimate the winter-average vertical ocean sensible heat flux (F_T) and the static stability of the upper water column via vertically-integrated (bulk) property distributions below the seasonal pycnocline (Figure S6). Static stability sets the barrier to overturn by surface buoyancy loss in winter and here is quantified by a bulk stability (Σ) (*26*). Figure 4 shows the 10-year mean (climatologies) for F_T and Σ.

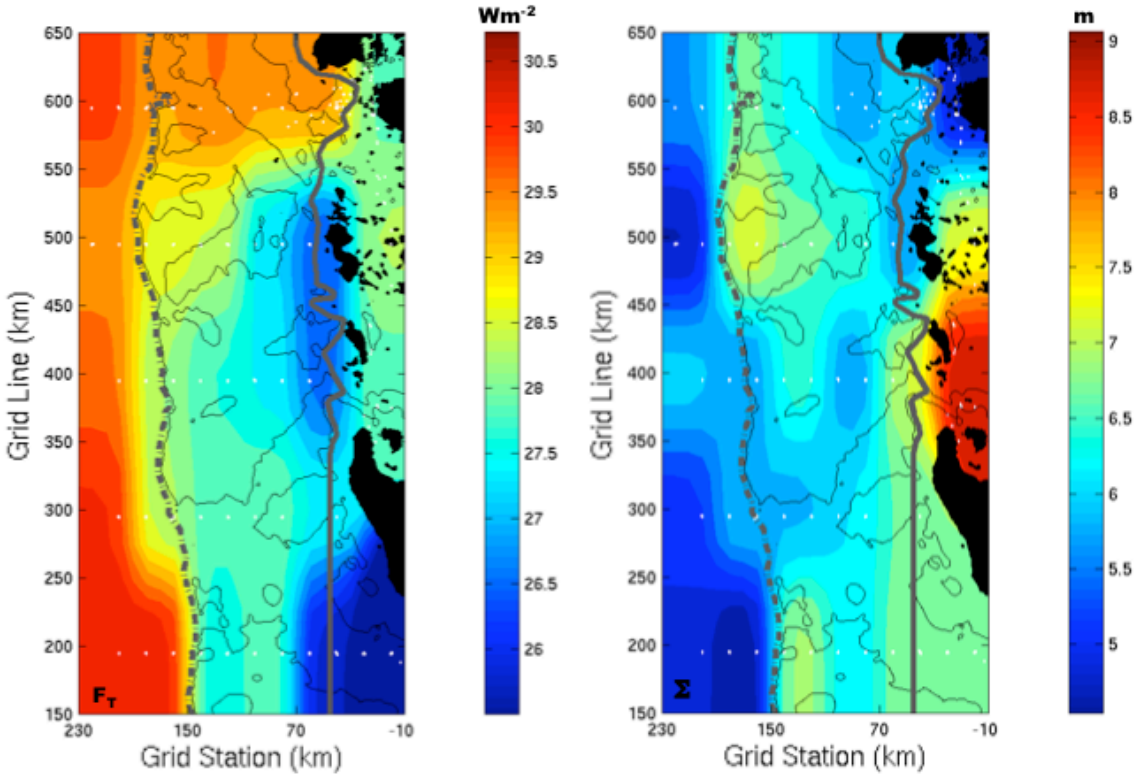

Figure 4: 10-year climatologies: (left) winter-average FT (Wm^{-2}), (right) □ (m of sea ice growth needed to eliminate permanent pycnocline in winter).

F_T averages ~28 Wm^{-2} across the sampling grid and is the sum of a weak turbulent diffusive flux and a much greater entrainment flux resulting from brine-driven thermocline erosion. F_T is sufficient to exhaust, in ~10 winters, all of the heat (relative to the freezing point) introduced by a typical ACC slope-water incursion; i.e., without renewal, warm deep waters on the shelf would cool to the freezing point in a decade. Even with continual renewal, it is possible to lose the heat through polynya formation following overturn (*25*).

Overturn occurs when sea ice growth rejects enough brine to overcome the bulk stability (*26*). A single winter's cooling could drive overturn during a year with an anomalously low Σ (*27*). This requires an $n\sigma_\Sigma$ event: $\Delta_o t \approx (\overline{\Sigma} - n\sigma_\Sigma)(\Sigma'_e - \dot{\Sigma}_t)^{-1}$ where σ_Σ is the interannual variability in Σ (here ±1m); n is the number of standard deviations about the mean; Σ'_e is the amount of bulk stability eliminated in a typical winter (with 5 months of winter surface cooling at an average rate of $\overline{F}_{air}$ = 35 Wm^{-2}, $\Sigma'_e \approx 1.5$m/yr); $\overline{\Sigma}$ is the mean bulk stability value at the location of interest; $\dot{\Sigma}_t$ is the temporal trend in Σ; and $\Delta_o t$ is the length of time in years until overturn is expected.

Attention is given to the Anvers region (Figure 3) since it shows minimal annual renewal of ACC slope-water (there: $\overline{\Sigma}$ ~6m and $\dot{\Sigma}_t \approx$ -0.22 m/yr). For n=0 (no anomaly about the mean value), it would take ~4 years until overturn. For any year with n≤–3.6, overturn would occur in a typical winter. Only one event of n≤–3.5 has occurred in ten years (2002), and at this rate overturn is expected in another 10 years. Because of the extreme magnitude of such an event, this time scale is also valid without the trend, $\dot{\Sigma}_t$ (i.e., even about the mean it produces a small

enough Σ), so that only the time scale of variability is important. Thus, ignoring other changes (e.g., in $\overline{F}_{air}$, or the circulation), overturn/polynya formation is likely within a decade.

Ocean heat is vented twenty times more efficiently through polynyas than through an ice cover, resulting in bottom water production. If the heat exhaustion occurs (via F_T) before overturn, sea ice growth will proceed unhindered, accelerating the destabilization of the water column and driving overturn. Bottom water production following overturn/polynya formation requires on-shelf flow to conserve mass: a self-regulating mechanism for preventing isolation of shelf waters from the warmer slope waters for more than a decade on average.

Shevenell and Kennett (S&K) (*15*) find evidence of decadal cycles (periods of cold, non-renewed shelf bottom waters alternating with warmer, renewed waters) recorded in their high-resolution sediment record from Palmer Deep (at Anvers Island). The self-regulating mechanism suggested above offers a means of recovering the on-shore flow of UCDW in the absence of larger scale atmospheric shifts as required in S&K's mechanism.

Regular flooding of the wAP continental shelf by ACC slope-water provides considerable heat to the local atmosphere and potentially to the base of marine glaciers (helping to fuel the wAP rapid warming and glacier retreat). *Rignot and Jacobs* (*12*) show that the rate of basal melting of glaciers near their grounding line increases by ~1 m/yr for each 0.1˚ C increase in water temperature above the freezing point of the *in situ* seawater. The ACC is delivering water to the coast at temperatures ≥3˚ C warmer than freezing, potentially driving tremendous melt rates. They also point out that the faster the warm water can be delivered, the greater the impact. The (at least) annual delivery reported here maintains a warm source close at hand, thus supplying the warm water as fast as any under-ice circulation allows.

If conditions change to reduce this on-shore delivery as in 1997 (Figure 3), the deep ocean heat would be vented in approximately a decade without renewal, replacing the shelf's warmer bottom water with cold water. If the heat is lost via a polynya, constant production of dense cold water will result in bottom water formation. This would drive a local onshore-offshore thermohaline circulation cell, pulling the warmer, stable offshore water back onto the shelf, stabilizing the water column, ending the polynya, and beginning a period of warm deep water again. This cycle of warm and cold bottom water, with its internal feedback capable of limiting the warm periods to about a decade, is consistent with modern and paleo-observations (*17,28*). This cycle impacts the extensive wAP ecosystems by supplying nutrients via the warm deep water (*17*).

With or without bottom water formation in the wAP region, there is considerable UCDW heat being vented to the atmosphere. Thus, the thermohaline circulation is still delivering a significant amount of heat to the subpolar Antarctic atmosphere, but it is not gaining additional bottom water formation for its trouble. This may change in the near future if current conditions and trends continue. Anecdotal reports of polynyas from field parties in the 1970s (*29*) suggest that overturn has occurred in this region in the recent past. Thus, it is not surprising to find that it is expected in the future. Paleoclimate data also suggests that the region was an area of bottom water formation during the last glacial period (*28*), consistent with polynya formation.

References/Notes:

1. D.G. Vaughan *et al.*, *Climatic Change* **60**, 243 (2003).
2. T.A. Scambos *et al., Geophys. Res. Lett.* **31,** (2004).
3. R. Thomas *et al.*, *Science*, **306**, 255 **(**2004).

4. E. Rignot *et al., Geophys. Res. Lett.* **31,** (2004).
5. S.E. Stammerjohn, R.C. Smith, in *Foundations for Ecological Research West of the Antarctic Peninsula*, R.M. Ross, E.E. Hofmann, L.B. Quetin, Eds. AGU, Washington, D.C., 81, (1996).
6. S.S. Jacobs and J.C. Comiso, *Geophys. Res. Lett.* 20, 1171 (1993).
7. S.E. Stammerjohn, personal communication.
8. J.H. Mercer, *Nature* **271**, 321 (1978).
9. E. Moris and D.G. Vaughan, *Ant. Res. Sci.* **79**, 61 (2003).
10. C.S.M. Doake and D.G. Vaughan, *Nature* **350**, 328 (1991).
11. T. Scambos, C. Hulbe, and M. Fahnestock, *Ant. Res. Sci.* **79**, 79 (2003).
12. E. Rignot, S.S. Jacobs, *Science*, **296**, 2020 (2002).
13. A. Shepherd, D. Wingham and E. Rignot, *Geophys. Res. Lett.* **31 (**2004).
14. R.C. Smith et al., in *Antarctic Peninsula Climate Variability*, Antarctic Research Series, **79**, 131, (2003).
15. A.E. Shevenell, J.P. Kennett, *Paleoceanography*, **17**, 10.1029/2000PA000596 (2002).
16. J. Turner et al., *Geophys. Res. Lett.* **29**, 10.1029/2002GL015565 (2002).
17. R.C. Smith *et al.*, *Oceanography*, **8**, 77 (1995).
18. A.H. Orsi, T. Whitworth III, and W. Nowlin, *Deep Sea Res.*, **42**, 641 (1995).
19. A.L Gordon, in *Antarctic Oceanology* I, T.L. Reid, Ed. (American Geophysical Union, Washington, D.C., 169, (1971).
20. R.G. Perkins and E.L. Lewis, J. *Ocean Engineering*, OE-5, #1, 9 (1980).
21. C.F. Guilivi and S.S. Jacobs, *Tech. Rep.* LDEO-97-03, 1997 (data available in NODC database)
22. ADCP observations (processed by Dr. Teri Chereskin) and dynamic topography maps (which show good agreement) reveal movement to the NE along the shelf/slope break, in agreement with velocity measurements farther south from Beardsley *et al*. (*24*), and absence of an eastwind drift.
23. J.F. Read, R.T. Pollard, A.I. Morrison, C. Symon, *Deep-Sea Res. II* **42**, 933 (1995).
24. R.C. Beardsley *et al., Deep Sea Res.*, in press.
25. D.G. Martinson, *J. Geophys. Res.*, **95,** 11641 (1990).
26. D.G Martinson, R.A. Iannuzzi, in *Antarctic Sea Ice: Physical Processes, Interactions and Variability,* M. Jeffries, Ed. (AGU), 243 (1998).
27. Materials and methods are available as supporting material on Science Online.
28. S.E. Ishman, and M.R. Sperling, *Geology*, **30**, 435 (2002).
29. W. Fraser, personal communication.
30. This work was supported by Palmer LTER NSF grant: VIMS #518603/1247, and leveraged by: NOAA grant UCSIO P.O. 10196097-003. 1993-1998 CTD data obtained via a Seabird SEACAT system incorporated into the Bio-Optical Profiling System (BOPS; Smith et al., 1997) instrument funded by NASA Grant #NAGW-290-n to R.C. Smith. Data analyses by R.A. Iannuzzi were fundamental. Discussions with S.E. Stammerjohn, S.S. Jacobs, M. Vernet, R.C. Smith, R.A. Iannuzzi, R. Ross, A.L. Gordon and T. Scambos have been invaluable. The National Ocean Data Center (NODC: http://www.nodc.noaa.gov/) and the Texas A&M online WOCE Southern Ocean database (http://woceatlas.tamu.edu/) allowed convenient access to historical data.

SUPPORTING ONLINE MATERIAL

Supporting Online Material
www.sciencemag.org
Materials and Methods
Figures S1, S2, S3, S4, S5, S6
References

Figure S1: Geographical Setting

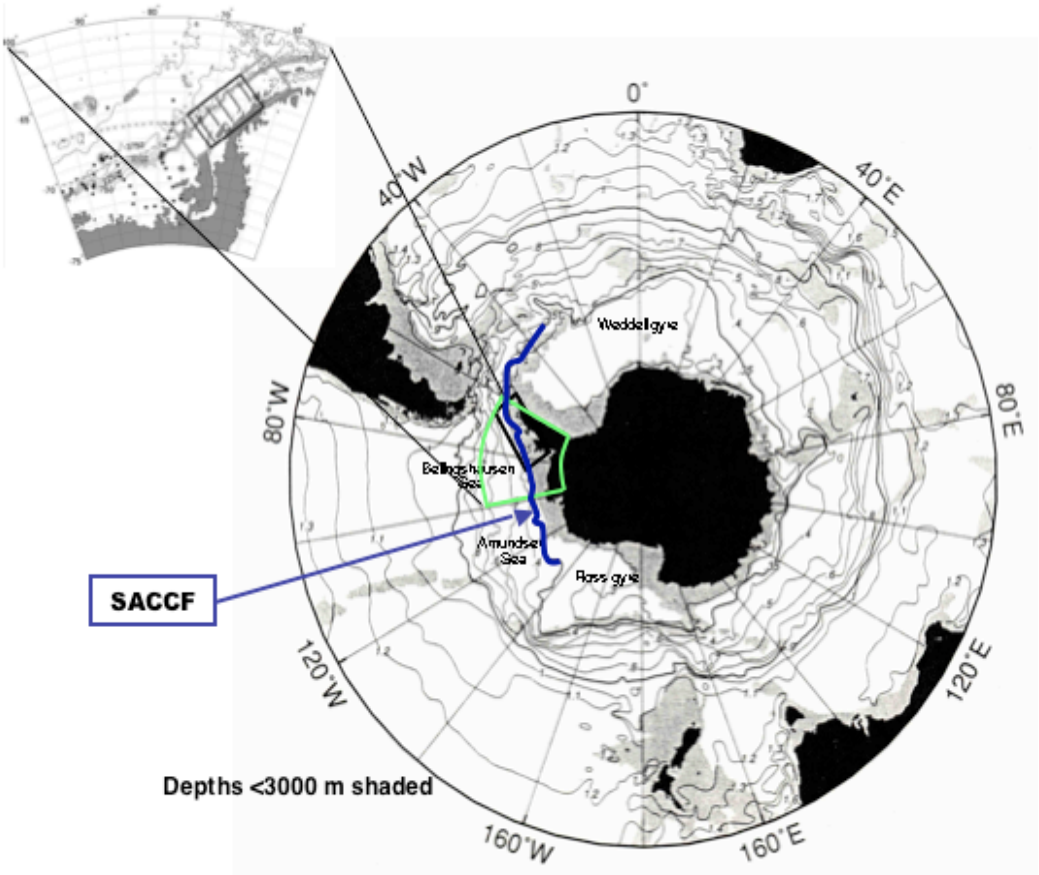

Figure S1: Location of LTER nominal sample grid (upper left inset). LTER has systematically sampled the wAP region since 1993. Most of the stations indicated in Figure 1B have been occupied each austral summer – typically the first week of January through mid-February. The LTER cruise data are supplemented and placed into a broader circumpolar context via comparison with hydrographical data collected throughout the Southern Ocean and primarily stored in the National Ocean Data Center (NODC: NBP94-02, small solid dots; Figure 1A) and Texas A&M University WOCE Southern Ocean online archives (of particular note: the WOCE S04P section across the southern Pacific; Figure 1A). Austral winter, spring and/or autumn data were collected during special process cruises (Nov. 1991, Mar. and Aug. 1993, Jul. 1999 and Sep. 2001). The analyses presented here are based upon 1315 CTD station profiles available from 13 separate cruises (1993-2002). A larger full grid, extending 200 km to the southwest and 300 km to the northeast represents the full LTER grid (bold grey box in upper left inset and Figure 1A), but it is too large to be sampled fully each year in the allotted ship time, thus the focus on this smaller imbedded nominal grid.

The nominal grid of Figure 1B predominantly overlies the broad continental shelf, averaging ~400 meters in depth and roughly 300 km in width. The glacially-sculpted (*S1*) coastline along the peninsula is highly convoluted, cut with numerous islands, deeps, bays, fjords, submarine canyons, and a series of embayments often interconnected by channels, sometimes as deep as 900 m. The domain is divided into three sub-regions (continental slope, shelf and coastal regions of Figure 1B) consistent with the bathymetry and ocean dynamics.

Figures S2 - S5: Water Mass Definitions/Descriptions

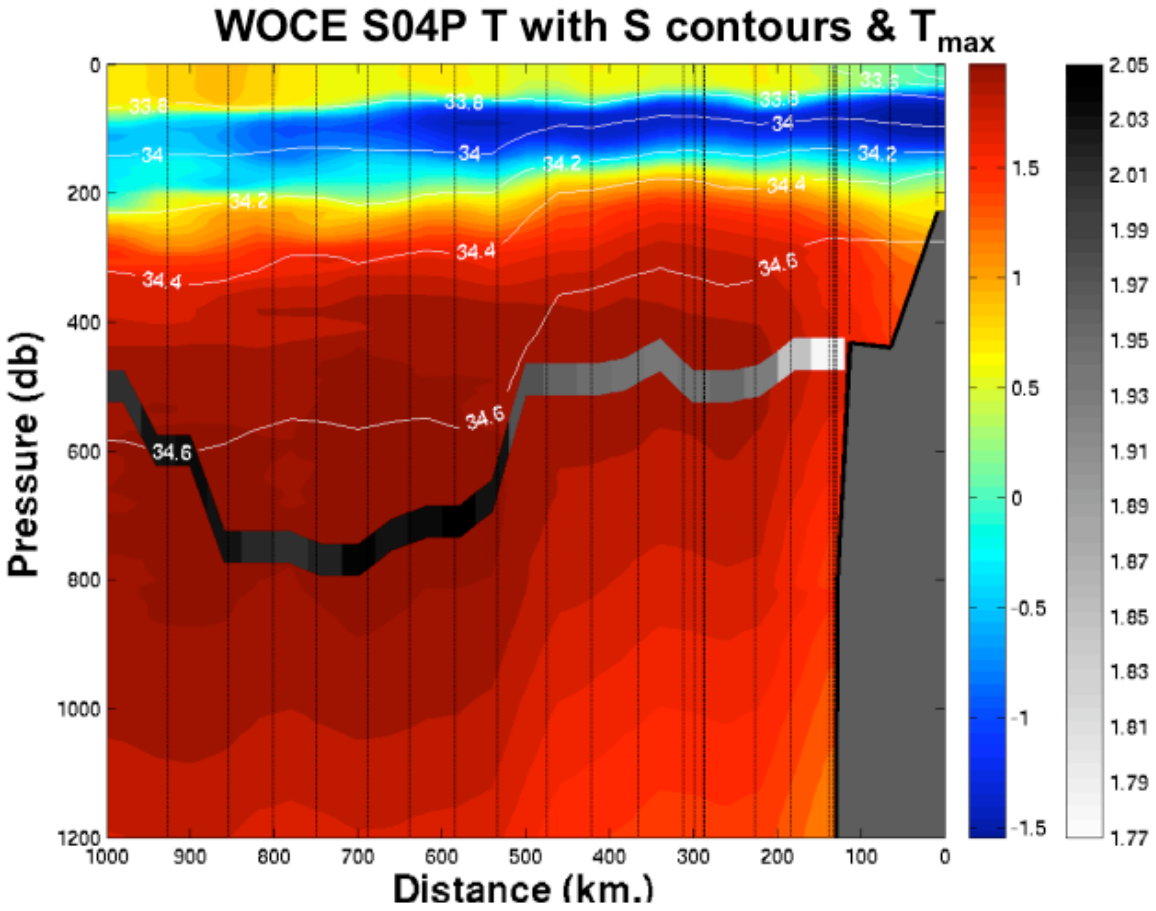

Figure S2: Temperature section from WOCE S04P line, from the LTER grid on the shelf (to the right of panel) extending 1000 km offshore (color bar to right shows section temperature). Depth and temperature of ACC-core UCDW (θ_{max}) indicated by grayscale band (grayscale bar at far right shows temperature of θ_{max} water). ACC-core UCDW terminates at the continental shelf/slope break, coinciding with the Southern ACC Front (SACCF) indicated by abrupt uplift of isopycnals (seen in the 34.6 isohaline contour). The same relationship between southern extent of the UCDW and SACCF is apparent in most of the LTER cross slope sections and hence are equated here, consistent with Read et al. (*S2*). Values in θ-S space are given in Figure S3.

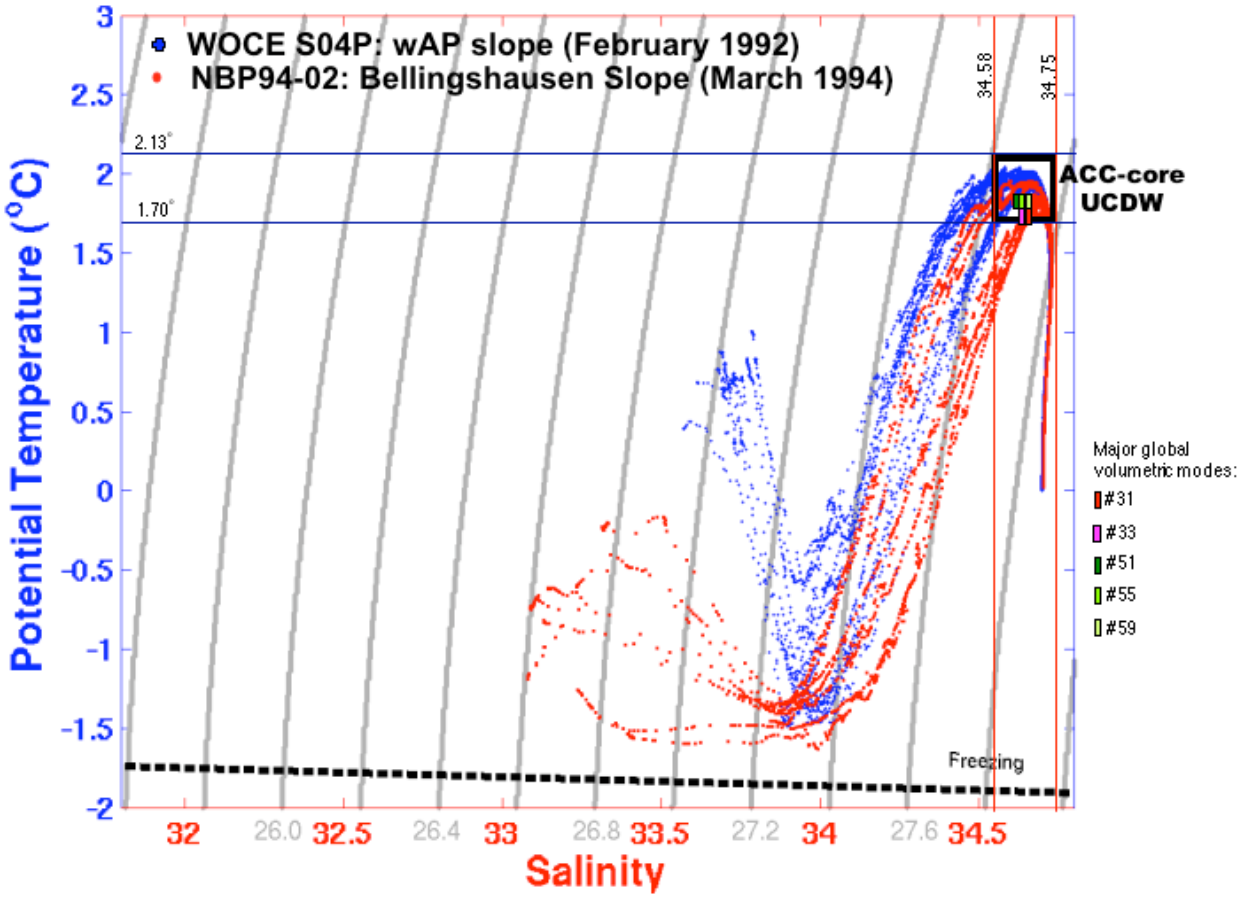

Figure S3: θ–S plot for the February 1992 WOCE S04P data (blue) lying within 1000 km of the wAP region in waters deeper than 3 km, and for March 1994 NBP94-02 data (red) on the slope in the Bellingshausen Sea (small dots in Figure 1A) showing values of regional ACC-core UCDW (as it appears off-shelf of the wAP). Within this box, are 5 small water classes (small areas in T-S space, following Montgomery, 1958 (*S3*)), lying within 0.1˚C x 0.01‰ boxes. Worthington (*S4*) shows that these classes represent major global ocean volumetric modes, helping further delimit the ACC-core UCDW definition. Specifically, of nearly 700 classes, those shown rank as: 31, 33, 51, 55 and 59 of the most voluminous water masses globally, as expected for CDW waters of the Southern Ocean. The bulk of the waters within these classes lie in the South Pacific, justifying their use in better defining the climatological regional variety of UCDW. This is necessary because the data used here span only 2 years.

Earlier studies have suggested that the ACC sweeps along the continental slope of the wAP region (*S5*-*S8*). This is consistent with the climatological southern limit of the ACC, as defined by *Orsi et al.* (*S7*) using the 0.35 geopotential height contour (Figure S1). Given the absence of current meter data during the years of LTER wAP observations, its location is quantified using *Orsi et al.'s* other definition, which is based on water mass distributions. Thus quantification of the water mass is required to locate the southern limit of the ACC in the wAP region.

Winter Water (WW; named by, and discussed at length by *Mosby* (*S9*)) is prevalent throughout the Antarctic polar waters (Figure S4); in the wAP it is found in austral summer as indicated in Figure 2A: $-0.8^{\circ}C \leq \theta \leq \theta_f$; $33.85 \leq S \leq 34.13$ (θ_f is freezing point). The water is formed at or very near the freezing point – being the remnant *winter* mixed layer water – but here the summer values are well above freezing due to vertical mixing with the warmer waters above

and below (*S10,S11*). Mixing across the overlying (seasonal) and underlying (permanent) pycnoclines serves to warm WW at a relatively rapid rate (approximately several milli-degrees per month for typical temperature profiles).

The most conspicuously absent Antarctic water masses on the wAP shelf are the low-and high-salinity shelf waters (LSSW, HSSW) found on the bottom of numerous shelf locations around the continent (*S12*). These waters, near the freezing point, with 34.6 salinity delimiting LSSW from HSSW, are notable for their role in deep and bottom water formation (*S13*). This absence is consistent with the notion that bottom waters do not form in the wAP region – a refreshing contrast to the humorous (but accurate in 1977) anecdote of *Jacobs and Georgi* (*S14*) who reported that "new source regions now seem to accumulate in rough proportion to the number of expeditions that reach the continental slope region".

In the wAP (and often elsewhere) the southern limit of UCDW and the Southern ACC Front (SACCF; southern limit of ACC indicated by abrupt shoreward uplift of the isopycnals) coincide (see Figure S2).

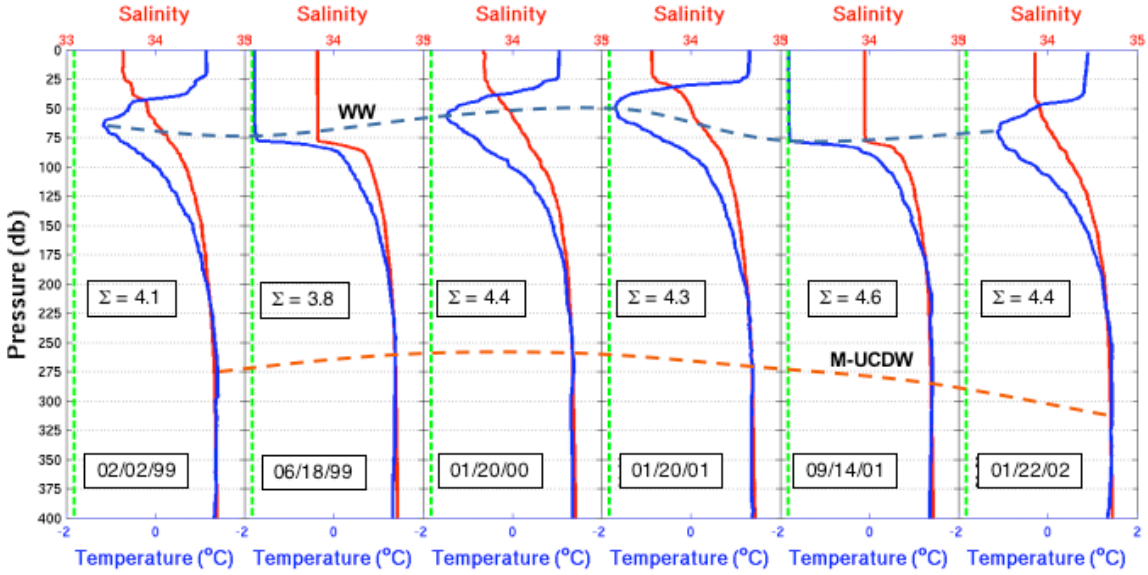

Figure S4: Location of primary Antarctic water masses on the continental shelf of the wAP (Winter Water, WW, dashed blue; and shelf variety of Upper Circumpolar Deep Water, M-UCDW; dashed red line) in profiles as they occur at the same location of the sampling grid (for adjacent seasons over 3 summers and 2 winters). Bulk stability (Σ), computed according to Martinson and Iannuzzi, (*S15*), agree to within 17% for June 1999 and January 2000, and to within 3% for September 2001 and January 2002, suggesting that the winter bulk parameter values can be estimated from summer profiles.

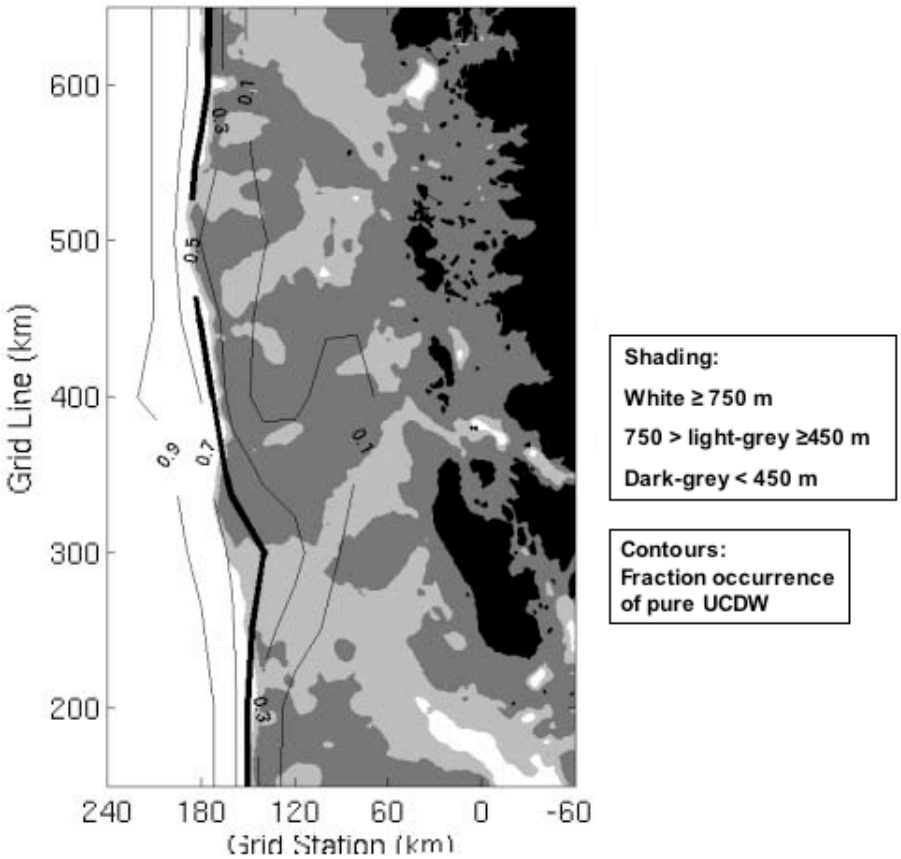

Figure S5: Fraction of January occurrences of ACC-core UCDW with shaded bathymetry labeled. Decadal mean position of SACCF is coincident with the 0.5 contour (bold line). Incursions of this water appear to enter primarily in the deep gap cut through the shelf into the slope between the 200 and 300 km lines (though this pattern is not apparent in the distribution of the ACC slope-water shown in Figure 3).

Figure S6: Bulk Property Methods

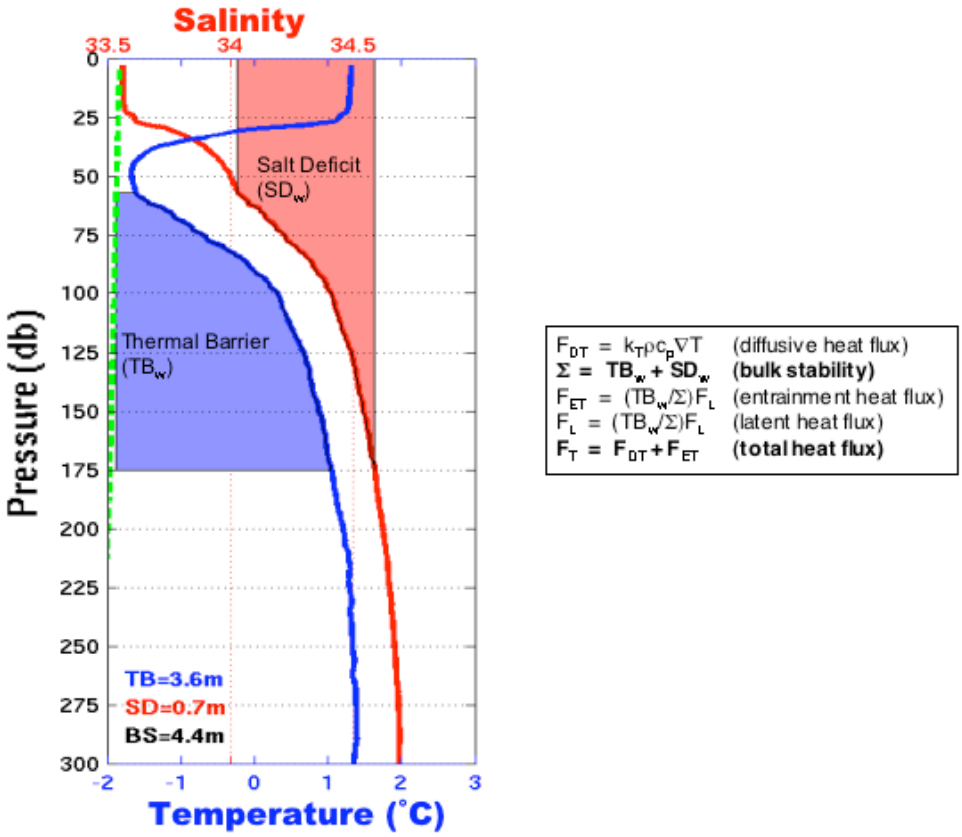

Figure S6: Graphical depiction of computation of bulk property estimates of winter-average vertical ocean sensible heat flux (F_T) and bulk stability (Σ) from a summer profile taken from Figure S3. Blue shaded region on temperature profile shows thermal barrier, and red shade area on salinity profile shows salt deficit. The bulk property parameters of Martinson and Iannuzzi (hereafter MI98) (*S15*) are adopted here. They utilize vertical integration of T and S profiles to provide bulk property distributions that are used directly, or in combinations, to provide fundamental ocean-atmosphere-ice information on ocean ventilation, water column stability and sea ice growth constraints. The parameters are based on the scalings of Martinson (*S16*), which quantify the primary regulation of the ocean-ice interaction as a robust function of the system's external parameters (mixed layer T, S and depth, and vertical gradients of temperature and salinity through the permanent pycnocline, ∇T and ∇S).

Two bulk properties dominate; others are derived from them. Foremost is the available thermal energy, presented here as a "thermal barrier" (TB_W). This is the enthalpy relative to the freezing point available within the permanent thermocline. Second is a winter "salt deficit" (SD_W). This is the freshwater surplus in the winter surface layer relative to the deep water (in terms of buoyancy, allowing for the nonlinear equation of state, vertical salt flux, etc.). SD_W must be eliminated by salt input in order to destabilize the surface layer, driving mixing with the underlying deeper waters during mixed layer expansion. TB_W is the sensible heat that must be vented during erosion of the pycnocline, accompanying complete elimination of SD_W. As it is vented, this heat stabilizes the water column by melting ice or, equivalently, by preventing ice

growth which would otherwise destabilize through brine rejection. Over seasonal time scales, for a vertically-driven system (as indicated for wAP by Klinck) (*S10*), SD_w is reduced by salinization during ice growth, driving an entrainment heat flux venting TB_w, and freshening and re-stabilizing (to some degree) the surface layer through ice melt. TB_w thus provides a negative feedback to the ice growth-driven destabilization process.

While buoyancy is the physical quantity of interest, these parameters are conveniently provided in terms of *in situ* sea ice growth, since that is the primary means of destabilization in winter and an easily measured or estimated observable in the field. As such, SD_w reveals the thickness of *in situ* ice growth required to reject enough salt to destabilize the surface layer. TB_w reveals the thickness of overlying ice that could be melted (or prevented from growing) by completely venting the thermocline, and it indicates the potential to resist overturn, usually dominating SD_w by a factor of 2-6 in Antarctic waters (Weddell gyre and wAP). The most notable combination of SD_w and TB_w occurs in the form of water column stability (Σ), where $\Sigma = TB_w + SD_w$. This measure of stability indicates the amount of *in situ* ice growth (or its heat loss equivalent) sufficient to drive overturn, ignoring storm influences or thermobaric effects, both shown to be of minor consequence in MI98.

Stability is the sum of both SD_w and TB_w because the destabilization induced by growing an amount of ice equivalent to SD_w will completely eliminate the thermocline, melting or preventing the growth of an amount of ice equivalent to TB_w. Thus, an additional amount of ice equal to TB_w must then grow in order to overcome the freshwater introduced by the melt (or its effective freshening by the prevention of ice growth).

The winter-average vertical ocean sensible heat flux (F_T) is composed of two parts from the ice-ocean interaction perspective: (1) a turbulent diffusive heat flux, estimated in the standard manner: $F_{DT} = \rho c_p k_T \nabla T$, where k_T is the turbulent diffusivity coefficient using 0.66×10^{-4} $m^2 s$; (2) an entrainment heat flux (F_{ET}) reflecting the sensible heat flux driven by erosion of the thermocline by mixed layer expansion during brine rejection from sea ice growth, where $F_{ET} = (TB_w/\Sigma)(\overline{F}_{air} - F_{DT})$. Total winter average vertical ocean heat flux, $F_T = F_{DT} + F_{ET}$.

Uncertainties in these values are evaluated at length in MI98 and shown to be small. All of these bulk parameters are readily determined from *summer* profiles. Computing the depth of convection when the surface layer is cooled to freezing in the autumn allows calculation of SD_w while ignoring the summer melt layer, assuming that the permanent pycnocline is essentially unchanged between summer and winter. These assumptions are shown to be reasonable by comparing summer values with those at the same stations in the following winter. Σ agrees to better than 83% (Figure S4) when estimating winter values from summer profiles.

The method works well in capturing the average winter heat fluxes — even in regions displaying significant lateral advection. For example, estimates of seasonally-averaged bulk parameter-derived heat fluxes for the central Weddell gyre region agree well with observed time-averaged values for the same location that were obtained using high-frequency sampling. Bulk property heat flux estimates for the 1994 Weddell ANZFLUX program (*S17*) are within 1 Wm^{-2} of the measured fluxes by McPhee et al. (*S18*). Note that F_T is a sensible (cooling) ocean heat flux, while the flux to the atmosphere is a combination of sensible and latent heat (ice formation) fluxes, so $F_{air} \neq F_T$.

Time scale until overturn calculation (text only)

The bulk stability near Anvers Island (and across much of the grid) is particularly low (≤4 m) in 2002. This is put into context by noting bulk stability values for other Antarctic continental shelf sites known to be regions of convection (bottom water formation). On the Weddell side of the AP, where bottom water formation does take place (*S19*), 2<Σ<4 m. In the Cape Adare region of the Ross Sea (feeding the Dryglaski Trough), where a program (AnSlope) is currently underway to monitor the shelf bottom water production and overflow known to occur there, the recent 266 summer shelf stations have $\overline{\Sigma}$=4.3 m (with 15 stations yielding values under 2 m and two with values ~1 m).

The rate (m/yr) at which bulk stability is eliminated in winter is $\dot{\Sigma}_e = (\rho_i L_i)^{-1}\overline{F}_{air}$ (i.e., the ice growth rate, for ice density, ρ_i = 900 kg/m^3; latent heat of fusion, L_i = 3.34x10^5 J/kg; average surface heat loss, $\overline{F}_{air}$ = 35 W/m^2, comparable to that measured in the Weddell region at comparable latitudes with slightly colder air temperatures, assuming 5% lead area in the sea ice). The amount of bulk stability eliminated in an average winter (say 5 months of cooling at $\overline{F}_{air}$) is Σ_e' ≈ 1.5 m/yr. To eliminate the bulk stability of Σ_{02} = 4 m (the 2002 value) would require ~3 winters of cooling at this rate. From a statistical perspective, assuming that the temporal trend in Σ continues at its present rate, $\dot{\Sigma}_t$ ≈ -0.22 m/yr, and the interannual variability remains σ_Σ = 1 m, then the amount of bulk stability elimination per year (Σ_e') is:

$$\overline{\Sigma}_e \Delta_o t = (\overline{\Sigma} - n\sigma_\Sigma) - \dot{\Sigma}_t \Delta_o t \qquad \text{S1}$$

or, the number of years until the bulk stability would be lowered (with ACC slope-water renewal) such that the water column would overturn within a typical 5 month winter is:

$$\Delta_o t = (\overline{\Sigma} - n\sigma_\Sigma)(\Sigma_e' - \dot{\Sigma}_t)^{-1} \qquad \text{S2}$$

where σ_Σ is the variability about the mean bulk stability ($\overline{\Sigma}$=6m).

References:

S1. J.B. Anderson, *Antarctic Marine Geology*, Cambridge University Press, Cambridge, UK (2002).

S2. J.F. Read, R.T. Pollard, A.I. Morrison, C. Symon, *Deep-Sea Res. II* **42**, 933 (1995).

S3. R.B. Montgomery, *Deep-Sea Res.* **5**, 134 (1958).

S4. L.V. Worthington in *Evolution of Physical Oceanography*, B.A. Warren, C. Wunsch, Eds. (MIT Press, Cambridge, MA, 1981), pp. 42-69.

S5. H.U. Sverdrup, *Discovery Reports 7, 139* (1933).

S6. A.L. Gordon, *Antarctic Oceanology I*, 169 (1971).

S7. A.H. Orsi, T. Whitworth III, and W. Nowlin, *Deep Sea Res.*, **42**, 641 (1995).

S8. E.E. Hofmann et al., *Antarctic Res. Ser.* **70**, 61 (1996).

S9. H. Mosby, *Scientific Results of the Norwegian Antarctic Expeditions 1927-1928*, **11**, 1 (1934).

S10. J.M. Klinck, *J. Geophys. Res.*, **103**, 7617 (1998).
S11. D.A. Smith, Ph.D. thesis, Old Dominion University (1999).
S12. E.C. Carmack in *A Voyage of Discovery, George Deacon 70th Anniversary Volume,* M. V. Angel, Ed., (Pergamon Press, Oxford, 1977), pp. 15-41.
S13. A.E. Gill, *Deep Sea Res.* **20**, 111 (1973).
S14. S.S. Jacobs, D.T. Georgi in *A Voyage of Discovery, George Deacon 70th Anniversary Volume,* M. V. Angel, Ed. (Pergamon Press, Oxford, 1977), 43-89.
S15. D.G Martinson, R.A. Iannuzzi, in *Antarctic Sea Ice: Physical Processes, Interactions and Variability,* M. Jeffries, Ed. (AGU, Boston, 1998), pp. 243-271.
S16. D.G. Martinson, *J. Geophys. Res.*, **95,** 11641 (1990).
S17. M.G. McPhee et al., *Bull. Amer. Met, Soc.*, **77**, 1232 (1996). S18. M.G. McPhee, C. Kottmeier, and J. Morison, *J. Phys. Ocean.* **29**, 1166 (1999).
S19. A.L. Gordon et al., *Science* **262**, 95 (1993).